Clinical Neurophysiology 138 (2022) 153–163

Contents lists available at ScienceDirect

Clinical Neurophysiology

journal homepage: www.elsevier.com/locate/clinph

Magnetoneurography as a novel functional imaging technique for the ulnar nerve at the elbow

Yuko Hoshino [a], Shigenori Kawabata [a,b,*], Yoshiaki Adachi [c], Taishi Watanabe [d], Kensuke Sekihara [a], Toru Sasaki [b], Jun Hashimoto [a], Koji Fujita [b], Akimoto Nimura [b], Atsushi Okawa [b]

[a] Department of Advanced Technology in Medicine, Graduate School of Tokyo Medical and Dental University, 1-5-45 Yushima, Bunkyo-ku, Tokyo 113-8510, Japan
[b] Department of Orthopedic Surgery, Tokyo Medical and Dental University, 1-5-45 Yushima, Bunkyo-ku, Tokyo 113-8510, Japan
[c] Applied Electronics Laboratory, Kanazawa Institute of Technology, Kanazawa-shi, Ishikawa 920-1331, Japan
[d] Healthcare Business Group, Ricoh Company, Ltd., 2-3-10 Kandasurugadai, Chiyoda-ku, Tokyo 101-0062, Japan

ARTICLE INFO

Article history:
Accepted 18 March 2022
Available online 30 March 2022

Keywords:
Evoked potential
Evoked magnetic field
Magnetoneurography
Magnetospinography
Recursively applied null-steering
Superconducting quantum interference device

HIGHLIGHTS

- Evoked magnetic fields of the ulnar nerve at the elbow were recorded by magnetoneurography.
- The neural activity of the ulnar nerve was visualized as reconstructed currents.
- Magnetoneurography is a novel functional imaging technique for the ulnar nerve.

ABSTRACT

Objective: To visualize the neural activity of the ulnar nerve at the elbow using magnetoneurography (MNG).
Methods: Subjects were asymptomatic volunteers (eight men and one woman; age, 26–53 years) and a male patient with cubital tunnel syndrome (age, 54 years). The ulnar nerve was electrically stimulated at the left wrist and evoked magnetic fields were recorded by a 132-channel biomagnetometer system with a superconducting quantum interference device at the elbow. Evoked potentials were also recorded and their correspondence to the evoked magnetic fields was evaluated in healthy participants.
Results: Evoked magnetic fields were successfully recorded by MNG, and computationally reconstructed currents were able to visualize the neural activity of the ulnar nerve at the elbow. In the affected arm of the patient, reconstructed intra-axonal and inflow currents attenuated and decelerated around the elbow. Latencies of reconstructed currents and evoked potentials were correspondent within an error of 0.4 ms in asymptomatic participants.
Conclusions: Neural activity in the ulnar nerve can be visualized by MNG, which may be a novel functional imaging technique for ulnar neuropathy at the elbow, including cubital tunnel syndrome.
Significance: MNG permits visualization of evoked currents in the ulnar nerve at the cubital tunnel.

1. Introduction

Cubital tunnel syndrome is a common peripheral nerve compression disorder at the elbow. It is generally diagnosed by neurological examination, an electrophysiological study, and imaging. Some authors have reported that cubital tunnel syndrome is progressive, although others consider it to have a more favorable outcome (Eberlin et al., 2017). However, untreated chronic cubital tunnel syndrome can lead to a permanent change in sensory and motor function and joint contracture (Boone et al., 2015).

Although a differential diagnosis including cervical nerve radiculopathy and brachial plexus pathology must be considered,

Abbreviations: CV, conduction velocity; MEG, magnetoencephalography; CMAP, compound muscle action potential; MNG, magnetoneurography; MSG, magnetospinography; RENS, recursively applied null-steering; SNAP, sensory nerve action potential; SQUID, superconducting quantum interference device; SD, standard deviation.

* Corresponding author at: Department of Advanced Technology in Medicine, Graduate School of Tokyo Medical and Dental University, 1-5-45 Yushima, Bunkyo-ku, Tokyo 113-8510, Japan.

E-mail addresses: hoshino.atm@tmd.ac.jp (Y. Hoshino), kawabata.orth@tmd.ac.jp (S. Kawabata), taishi.watanabe@jp.ricoh.com (T. Watanabe), k-sekihara@nifty.com (K. Sekihara), fujiorth@tmd.ac.jp (K. Fujita), nimura.orj@tmd.ac.jp (A. Nimura), okawa.orth@tmd.ac.jp (A. Okawa).

https://doi.org/10.1016/j.clinph.2022.03.017
1388-2457/

the diagnosis of cubital tunnel syndrome is typically not difficult. Nonetheless, some patients with cubital tunnel syndrome present normal electrophysiological findings. Greenwald et al. reported that electromyography and nerve conduction velocity (CV) studies may have false-negative rates exceeding 10% in patients presumed to have clinical cubital tunnel syndrome. They considered that this might be because very few axons need to be functional for the study to be interpreted as normal (Greenwald et al., 2006). Beekman et al. pointed out that electrodiagnostic studies of ulnar neuropathy at the elbow may obtain false-negative results, particularly in patients with milder lesions. In addition, they reported that nerve enlargement in sonography was related to an abnormal electrophysiological test and that the sensitivity of the examination increased using both modalities (Beekman et al., 2004). Pelosi et al. (2018) reported that ulnar neuropathy with abnormal non-localizing electrophysiology was not uncommon. They showed that nerve ultrasound could identify the local lesion at the elbow in the majority of such cases.

Furthermore, there has been controversy regarding the treatment option for cubital tunnel syndrome. A more precise functional imaging technique may contribute to new insights into the pathology and prognosis of cubital tunnel syndrome.

Magnetoneurography (MNG) is a new functional imaging method for the nervous system that records magnetic fields generated according to the Biot–Savart law or Ampère's law after electrical nerve stimulation. One of the most valuable features of MNG is that it can reconstruct and visualize currents inside and outside of the nerve. Given that traditional electrophysiological studies evaluate only evoked potentials, MNG could contribute not only to clinical examination, but also to novel physiological findings.

The development of MNG for the spinal cord and peripheral nerves has been gradual compared with magnetoencephalography and magnetocardiography, mainly owing to the anatomical features of these nerves (Mackert, 2004; Afra, 2020). We previously developed a magnetospinography (MSG) system that enables an examination of the spinal cord and peripheral nerves (Fukuoka et al., 2002, 2004; Kawabata et al., 2002; Hoshino et al., 2005; Tomizawa et al., 2008; Ishii et al., 2012; Sumiya et al., 2017; Sasaki et al., 2020; Ushio et al., 2019; Watanabe et al., 2019).

In this article, we show that MNG can visualize the neural activity of the ulnar nerve around the medial epicondyle. In addition, we report that it has the potential to be a novel functional imaging technique that can identify subclinical electrophysiological abnormalities and localized lesions in unconfirmed cases of ulnar neuropathy at the elbow.

2. Methods

2.1. MSG system

Biomagnetic signals were recorded in a magnetically shielded room with a 132-channel superconducting quantum interference device (SQUID) biomagnetometer system developed by the Kanazawa Institute of Technology and Ricoh Company, Ltd. (Adachi et al. 2017). The system has 44 vector-type SQUID magnetic sensors arranged in a 180-mm × 130-mm area along a cylindrical surface with a radius of 200 mm (Fig. 1). Each sensor has three pick-up coils orthogonally facing each other, which record magnetic fields from three orthogonal directions (X-, Y-, and Z-coils).

2.2. Positional information

Before the recording, two marker coils were placed under the subject's upper extremity and a lateral X-ray image was obtained (Fig. 2). The relative positions of the marker coils to the MSG sensors were estimated from magnetic fields generated by the marker coils. Subsequently, the subject's position on the recording area was obtained.

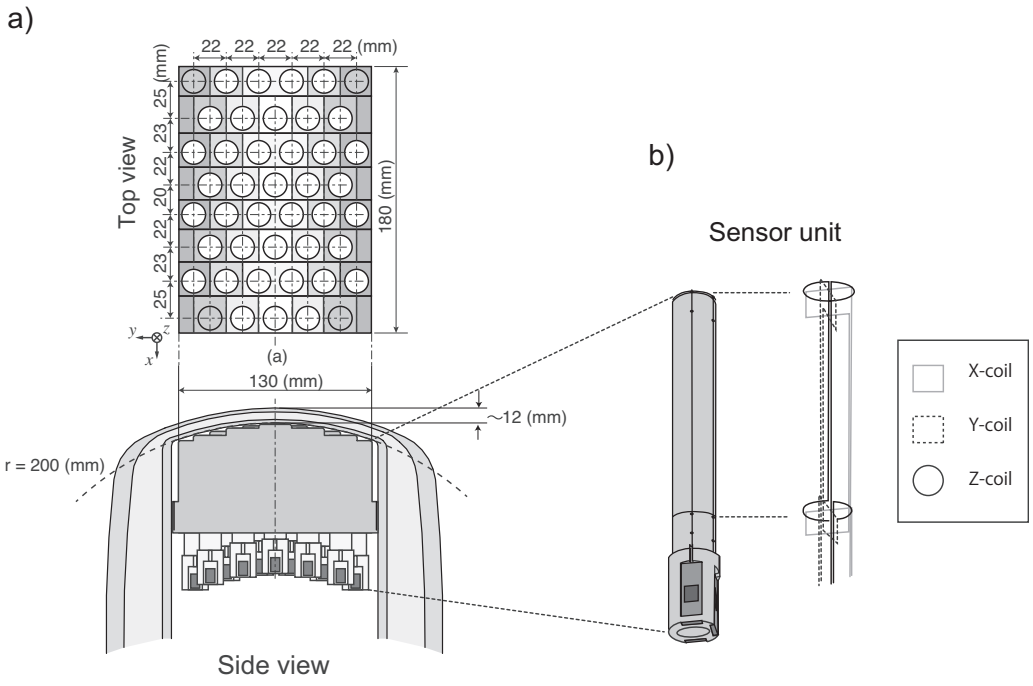

Fig. 1. Structures of the magnetoneurography (MNG) system and sensor units. (a) Side and top views of the MNG sensor array. It consists of eight columns, which each have five or six sensor units. The four sensor units at the four corners have only one channel for positional information and each of the other 40 sensor units have three channels for recording three-directional magnetic fields (X-, Y-, and Z-coils in Fig. 1b). This Figure is reproduced with permission from the reports of Adachi et al. (2017) (©2017 IEEE. Reprinted with permission from https://doi.org/10.1088/1361-6668/aa66b3) and Sasaki et al. (2020).

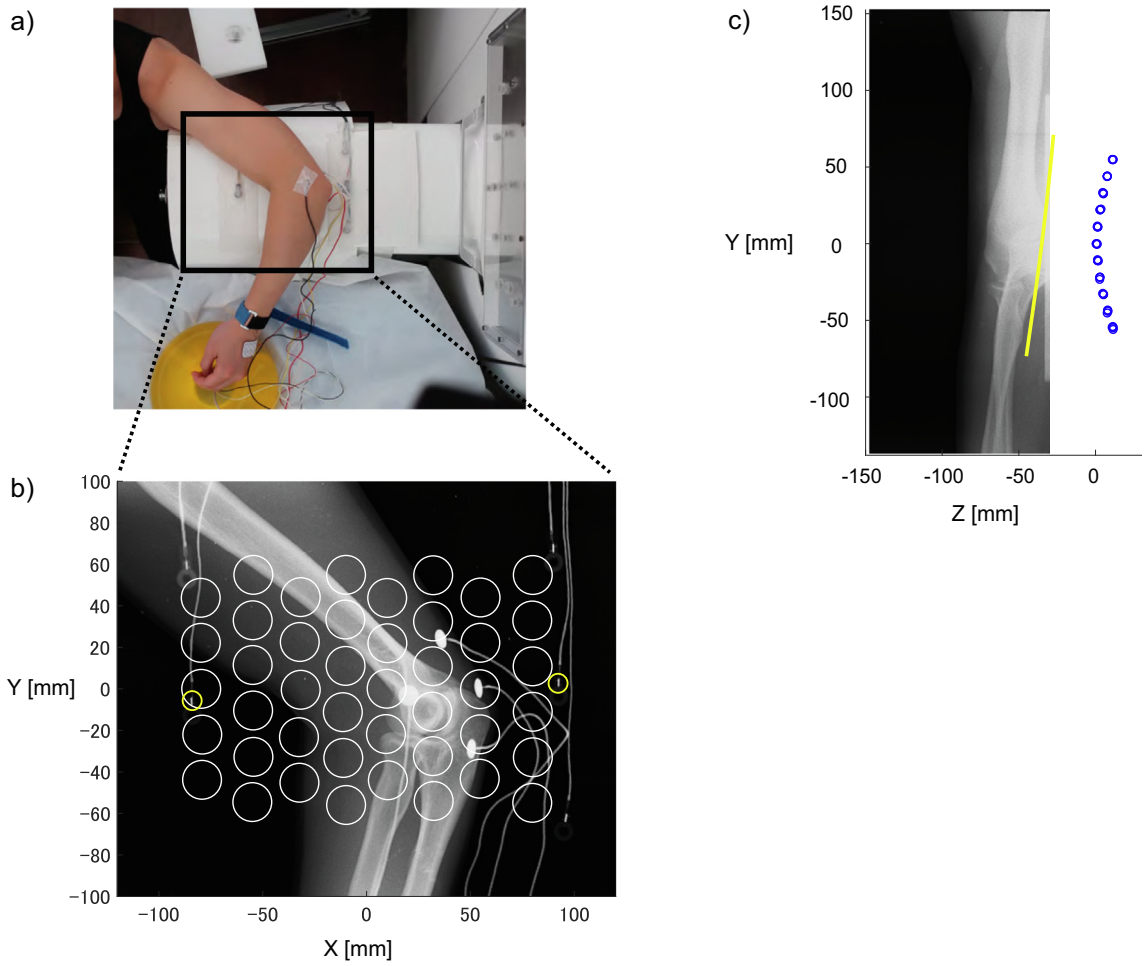

Fig. 2. Recording setting and acquisition of positional information. (a) Although there are five marker coils on the sensor wall, two were used to acquire positional information. The black box shows the area of the X-ray image. (b) X-ray image and sensor array. White circles represent sensors and there are three electrodes for recording evoked potentials and one for a reference near the elbow joint. Two marker coils marked with yellow circles were used for positional information. (c) The yellow line represents the depth of the region of interest (ROI). The line passes through the cubital tunnel and is parallel to the ulnar margin of the humerus and the ulna. Blue circles represent the positions of sensors. (For interpretation of the references to colour in this figure legend, the reader is referred to the web version of this article.)

2.3. Participants and recordings of evoked potentials and magnetic fields

The subjects were nine asymptomatic volunteers without any history of neurological disease (eight men and one woman; age, 26–53 years) and one male patient with left cubital tunnel syndrome (age, 54 years). The patient presented with a 1-year history of numbness of the left little finger but did not show muscle atrophy. He underwent subcutaneous anterior transposition of the ulnar nerve, and the numbness in the left little finger had almost disappeared 9 months after the surgery. For the recordings of neuromagnetic fields and nerve action potentials in the healthy participants, the ulnar nerve was electrically stimulated at the left wrist with a supramaximal intensity that evoked maximal sensory nerve action potential (SNAP) at the little finger (5 Hz; monophasic square waves, 0.3-ms width). Evoked magnetic fields were recorded by the MSG system with the subject seated using a 40-kHz sampling rate and a 100–5000-Hz bandpass filter (Fig. 3). About 2000 responses (2000–2126) were averaged. The MNG examination time was about 15 min per individual.

For the healthy participants, nerve action potentials were recorded at three points at the left elbow: just above the medial epicondyle and 3 cm proximal and 3 cm distal to the medial epicondyle (10-kHz sampling rate; 20–2000-Hz bandpass filter). The CV of the nerve action potential was calculated from the difference in latencies at two points: 3 cm proximal and 3 cm distal to the medial epicondyle.

Because the electrophysiological examination of the patient was performed at a hospital, his recording setting was different from that of the healthy participants. For the patient, the little finger of each side was electrically stimulated, and SNAPs were recorded at the wrist, distal and proximal points of the medial epicondyle, and axilla. Compound muscle action potentials (CMAPs) of the abductor digiti minimi were also recorded in response to electrical stimulation of the ulnar nerve at the wrist, distal and proximal points of the medial epicondyle, and axilla. Before surgery, a neuromagnetic recording of the patient was conducted in the same manner as in the healthy participants. Electrical stimulation and recordings were performed by the MEB2200 electromyogram/evoked potential measuring system (Nihon Koden, Tokyo, Japan).

All procedures in this study were approved by the Ethics Committee of Tokyo Medical and Dental University and carried out in accordance with the Declaration of Helsinki. We obtained written informed consent and releases for images and photographs from all participants.

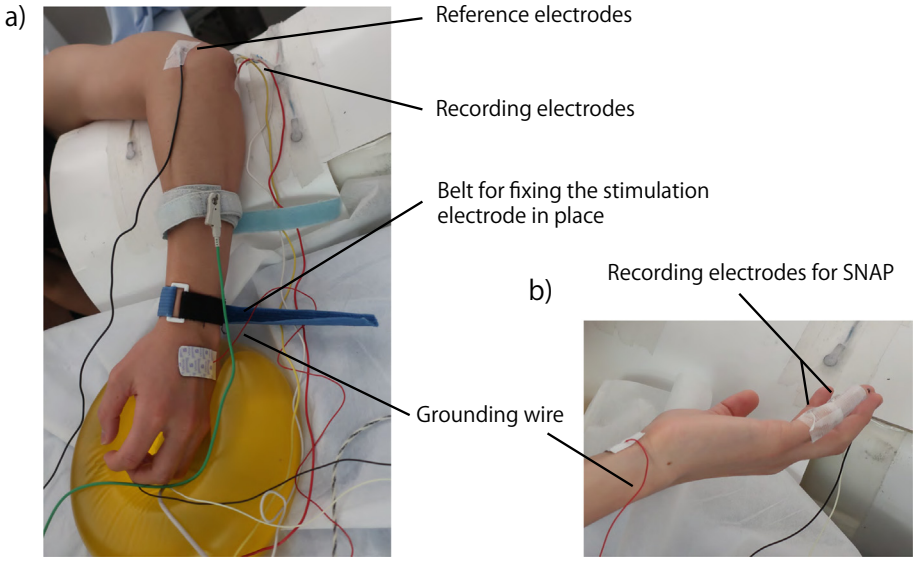

Fig. 3. Recording setting of evoked potentials. (a) Evoked potentials were recorded at three points along the left cubital tunnel (10-kHz sampling rate; 20–2000-Hz bandpass filter) in response to electrical stimulation of the ulnar nerve at the left wrist (5 Hz; monophasic square waves, 0.3-ms width). (b) Electrical stimulation at the wrist was at a supramaximal intensity that evoked maximal sensory nerve action potential at the little finger.

2.4. Signal processing

Recorded magnetic fields were first processed using an artifact reduction method, the dual signal subspace projection (DSSP) algorithm (Sekihara et al., 2016, Sekihara and Nagarajan, 2017). Then, the positions and intensities of current sources were reconstructed from the processed data using a spatial filter algorithm, the recursively applied null-steering (RENS) beamformer (Kumihashi and Sekihara, 2010; Sekihara and Nagarajan, 2015). The depth of the region of interest (ROI) was set at the pathway of the ulnar nerve, which was assumed to run through the posterior of the medial epicondyle and to be parallel to the ulnar margin of the humerus and the ulna in an anteroposterior X-ray image (yellow line in Fig. 2c). This procedure allowed reconstruction of the evoked current at an arbitrary point on the plane at the ROI as if a virtual electrode were placed there.

To evaluate the CVs of reconstructed currents and the correspondence between them and evoked potentials, the assumed conduction pathway was set at the peak of reconstructed currents selected computationally. CVs of intra-axonal currents and currents perpendicularly flowing toward the conduction pathway were respectively calculated from the latencies at the points 3 cm proximal and 3 cm distal to the tip of the medial epicondyle. Regarding the influent currents, waveforms from the virtual electrodes 10, 15, and 20 mm away from the conduction pathway were evaluated. The peak latencies of evoked potentials and reconstructed currents nearest to the medial epicondyle were evaluated to assess correspondence.

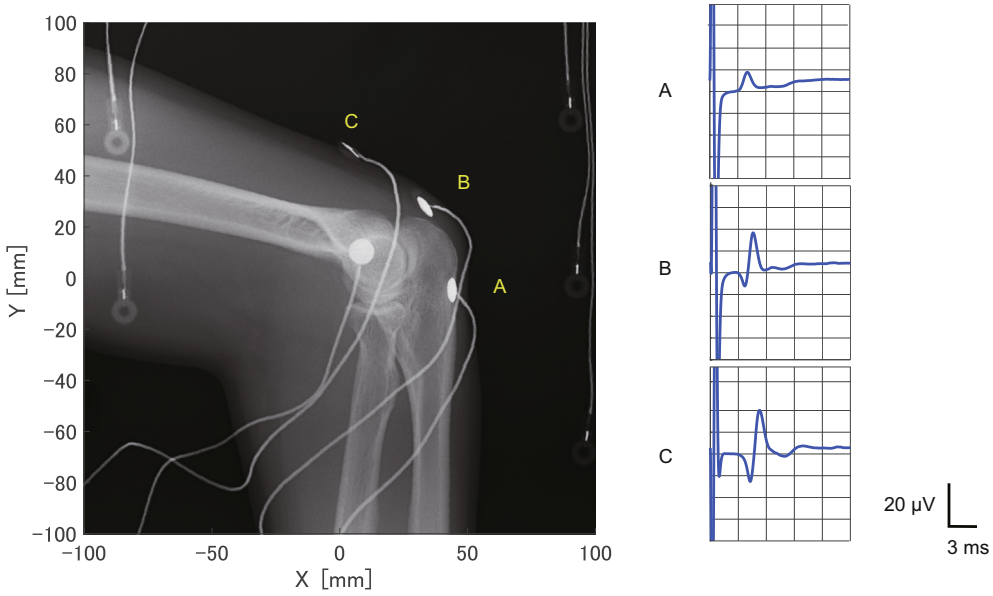

Fig. 4. Evoked potentials in response to electrical stimulation of the ulnar nerve at the left wrist. Evoked potentials were recorded at three electrodes around the cubital nerve. B is at the cubital tunnel. A and C are 3 cm distal and 3 cm proximal to B. Evoked potentials propagated from distal to proximal.

3. Results

3.1. Recording of evoked potentials

In all participants, evoked potentials were recorded after stimulation of the left ulnar nerve (Fig. 4). The upward peak of the waveform propagated from the distal to proximal electrodes. The mean CV of the evoked potentials was 61.2 ± 9.8 m/s (mean ± standard deviation [SD], n = 9). The same healthy subject and the patient are shown in Figs. 4–10.

In the patient with left cubital tunnel syndrome, the CVs of the SNAPs between the distal and proximal points of the medial epicondyle were 59.5/30.1 m/s (right/left) and 58.1/55.6 m/s (right/left) before and after the surgery, respectively. Similarly, the CVs of the motor nerve were 52.6/31.7 m/s and 57.1/50.0 m/s, respectively. The SNAP in the left arm was attenuated and decelerated around the cubital tunnel (pink arrowheads in Fig. 5a). Note that the scale of the amplitude in the left arm before surgery is much smaller than in other recordings. Similarly, the motor nerve conduction decelerated near the cubital tunnel (pink arrowheads in Fig. 5b).

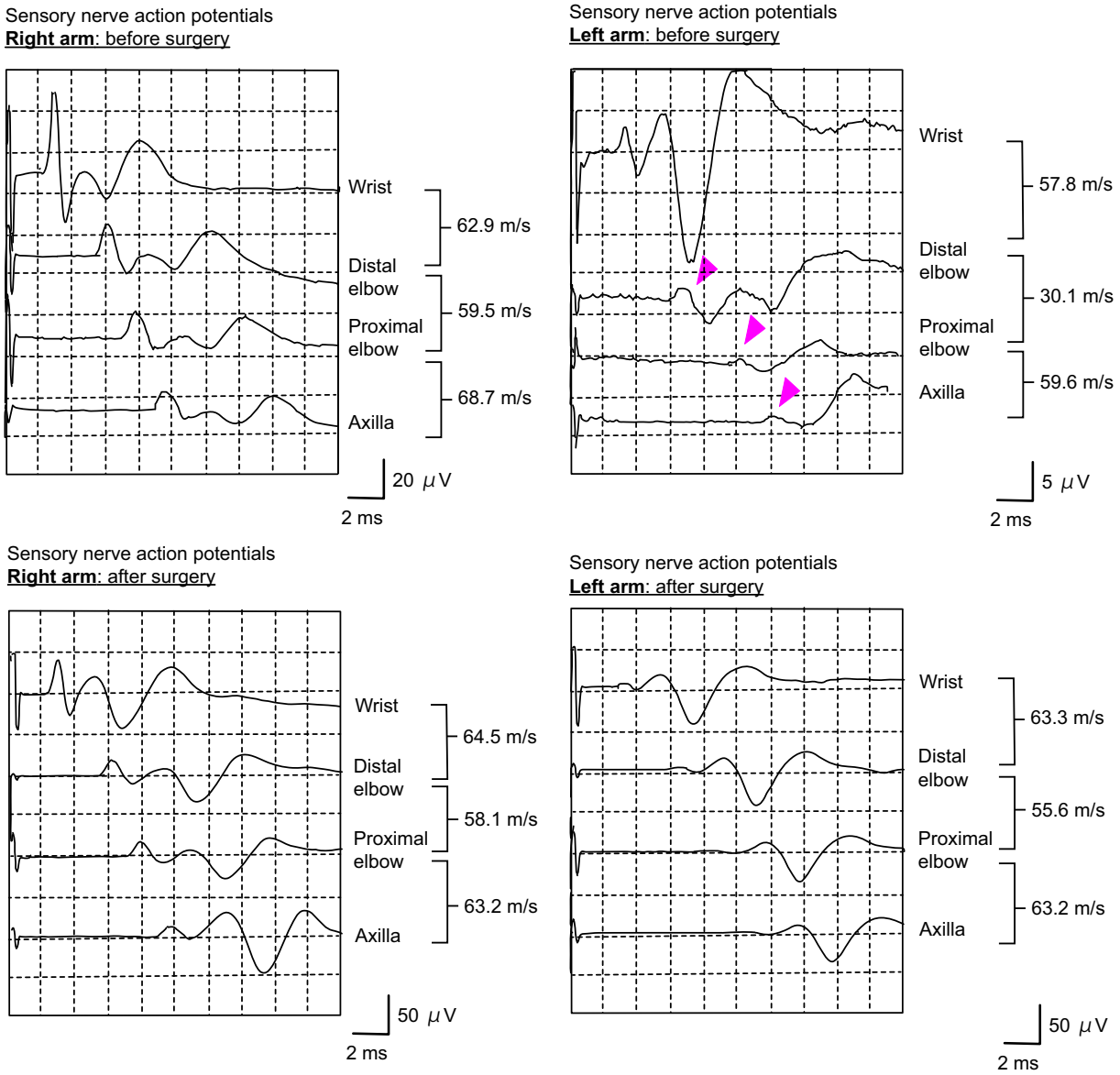

Fig. 5. Electrophysiological studies of a patient with left cubital tunnel syndrome. (a) Sensory nerve action potentials (SNAPs) in response to electrical stimulation of the digital nerve at the little finger. SNAPs of the right and left arms were recorded at the wrist, distal and proximal points of the medial epicondyle, and axilla. Distances between each recording point are not constant. Conduction velocities are shown on the right side of the charts. Upper row: SNAPs before surgery. On the affected side (left arm), the propagation of SNAPs attenuated and decelerated around the elbow (pink arrowheads). Lower row: The deceleration of SNAPs in the left arm improved after surgery. (b) Compound muscle action potentials (CMAPs) of the abductor digiti minimi in response to electrical stimulation of the ulnar nerve recorded at the wrist, distal and proximal points of the medial epicondyle, and axilla. Upper row: CMAPs of the right and left arms before surgery. Conduction velocities between two recording points are shown on the right side of the charts. On the affected side (left arm), the propagation of CMAPs attenuated and decelerated beyond the medial epicondyle (pink arrowheads). Lower row: CMAPs after surgery show that the conduction in the left arm recovered compared with before surgery. (For interpretation of the references to colour in this figure legend, the reader is referred to the web version of this article.)

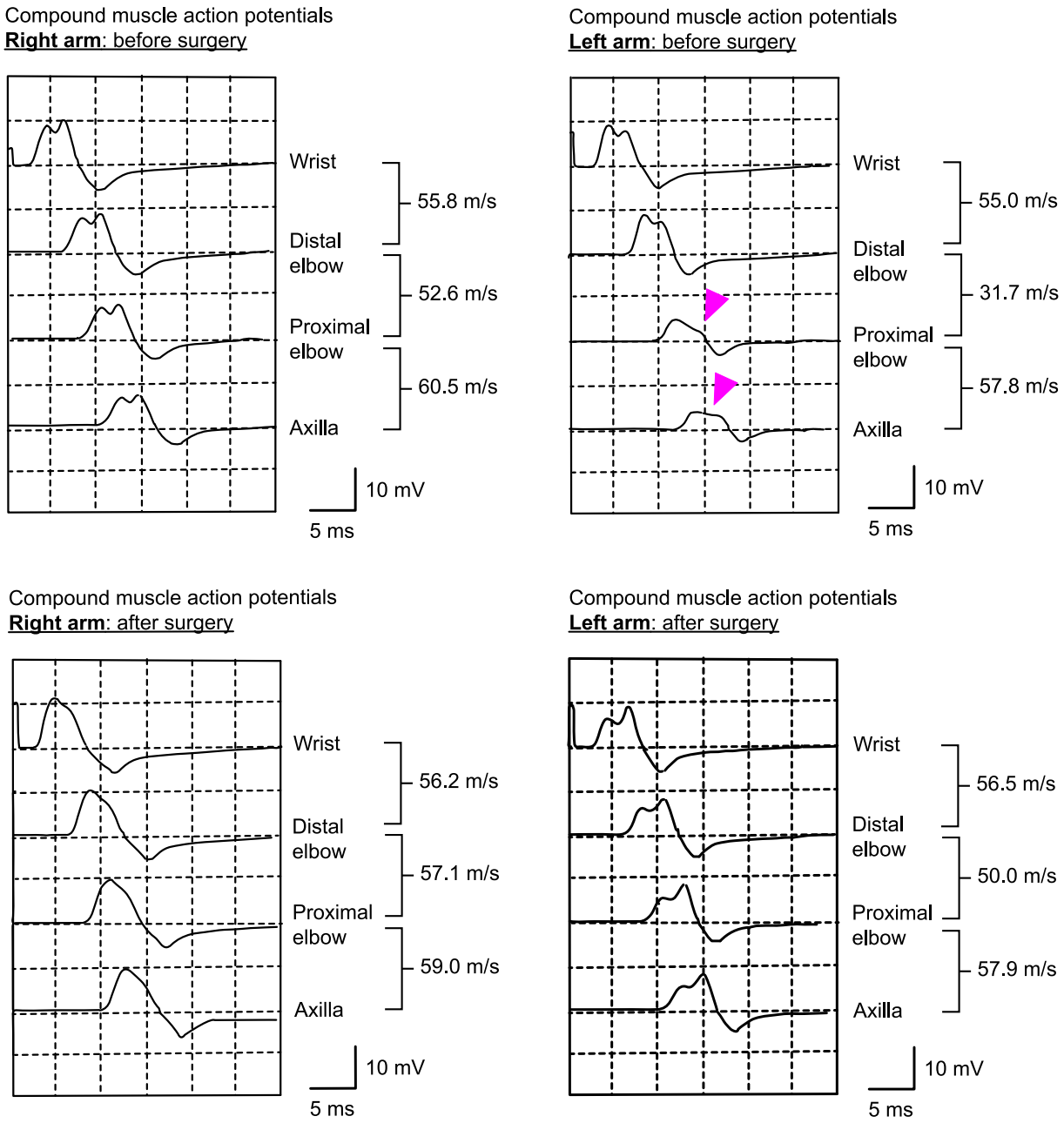

Fig. 5 (*continued*)

3.2. Recording of evoked magnetic fields

In all subjects, evoked magnetic fields were recorded in response to the electrical stimulation. In Fig. 6, the evoked magnetic fields are superimposed on the X-ray image. In the recording setting, the elbow and the ulnar nerve are above the sensor. Polarity is reversed between the two sides of the assumed position of the ulnar nerve (pairs of colored stars in Fig. 6).

3.3. Reconstructed current distribution

The equivalent currents reconstructed by the RENS beamformer are illustrated in a pseudocolor map and superimposed on the X-ray image (Fig. 7). From 3.5 ms to 6.3 ms, high-intensity currents flowing toward the head appeared near the electrodes for evoked potentials and conducted proximally (pink stars in Fig. 7). In addition, there were currents flowing toward the end of the above-described currents and also conducting proximally (yellow arrows in Fig. 7). From 4.9 ms to 7.0 ms, currents directing caudally appeared and conducted proximally (yellow stars in Fig. 7).

The CV of the intra-axonal reconstructed currents was 60.8 ± 5.6 m/s (mean ± SD, n = 9). As described in Section 2.4, perpendicularly flowing currents 10, 15, and 20 mm away from the conduction pathway of the intra-axonal currents were reconstructed and their suitability evaluated. The CVs of these currents were 62.5 ± 16.6 m/s, 60.3 ± 9.1 m/s, and 60.1 ± 9.0 m/s (mean ± SD, n = 9), respectively.

We evaluated the differences between the peak latencies of evoked potentials and reconstructed inflow currents near the cubital tunnel. For the reconstructed currents 10, 15, and 20 mm away

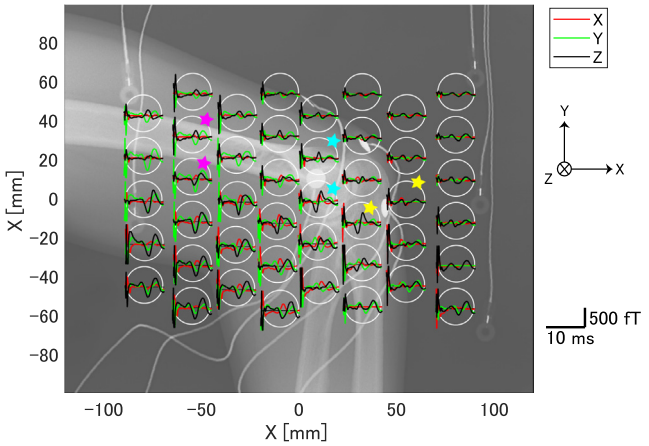

Fig. 6. Evoked magnetic fields of a representative case. Evoked magnetic fields recorded from each sensor are superimposed on the X-ray image. White circles represent sensors. Red waveforms show magnetic fields recorded from X coils, with upward positive in the X-axis; green waveforms are from the Y coil, with upward positive in the Y-axis; and black waveforms are from the Z coil, with upward positive in the direction toward the floor. Polarity is reversed between either side of the assumed position of the ulnar nerve (marked with colored stars). (For interpretation of the references to colour in this figure legend, the reader is referred to the web version of this article.)

from the conduction pathway, the differences were 0.058 ± 0.34 ms, −0.011 ± 0.29 ms, and −0.031 ± 0.25 ms, respectively ([evoked potential] − [reconstructed current]; mean ± SD, n = 9). We thus chose data at the position of 15 mm away for the consistency evaluation (described below) because it showed the lowest difference. Time courses of intra-axonal currents and inflow currents 15 mm away from the conduction pathway are shown in Fig. 8b. The correspondence between the waveforms of the evoked potentials and reconstructed inflow currents is shown in Fig. 8c. In the representative subject shown in Fig. 8, the differences in the peak latencies at three points around the medial epicondyle (A & 2, B & 4, and C & 6 in Fig. 8c) were −0.005, 0.045, and −0.165 ms, respectively.

In the patient with cubital tunnel syndrome, reconstructed intra-axonal and inflow currents propagated along the ulnar nerve on the right intact side (yellow and pink arrowheads in Fig. 9a). In contrast, these currents disappeared after 5.0 ms in the left arm (yellow arrowheads in Fig. 9b).

The reconstructed intra-axonal and inflow currents propagated cranially in the right elbow (Fig. 10a) and the CVs were 50.1 m/s and 48.2 m/s, respectively. However, the upward pointed waves seen in the intra-axonal currents were not clear in the left arm (affected side), and the inflow currents decelerated and attenuated near the medial epicondyle (electrodes 5–7 in Fig. 10b). Note that the scale of the amplitude on the left side is one-fifth that on the right side. The CVs of the intra-axonal reconstructed currents could not be calculated. The inflow currents propagated up to the distal point of the medial epicondyle at a CV of 48.3 m/s (calculated from electrodes 3–5).

4. Discussion

The development of the MNG technique has recently been progressing due to refinements of the recording system. One of the advantages of MNG is that it can visualize neural activity as reconstructed currents. In the healthy participants, the CVs of evoked potentials recorded above the medial epicondyle and of reconstructed currents flowing toward the conduction pathway from 15 mm away were similar: 61.2 ± 9.8 m/s (mean ± SD, n = 9) and

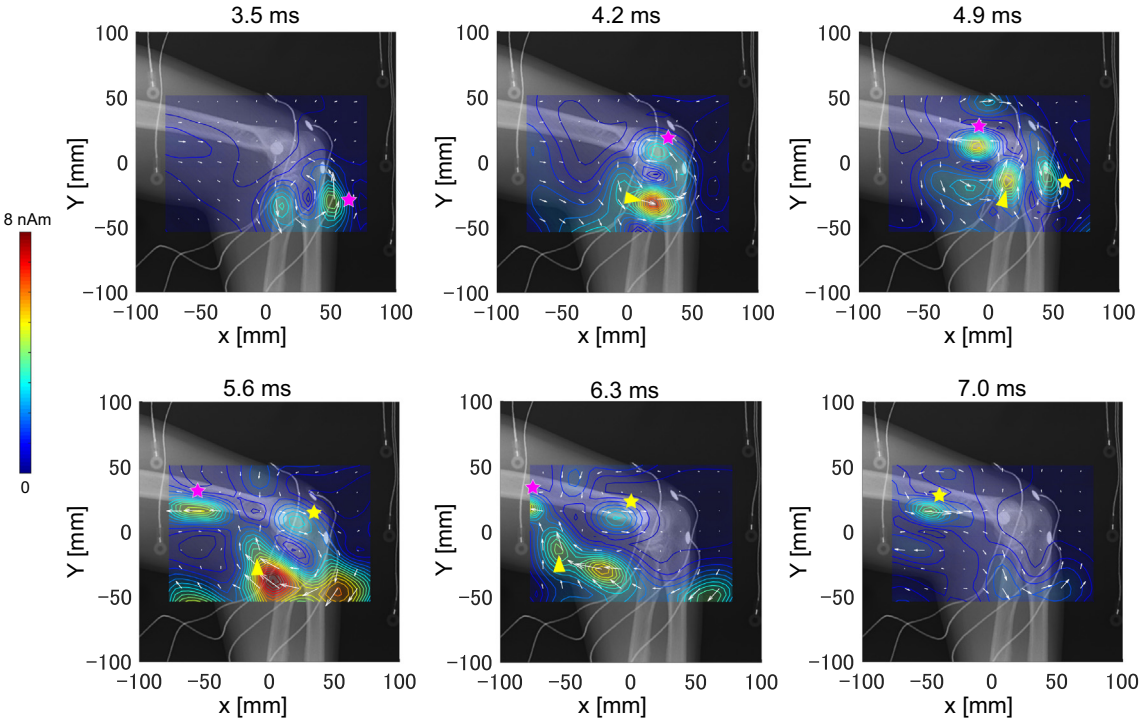

Fig. 7. Spatiotemporal changes in equivalent currents reconstructed with the recursively applied null-steering (RENS) beam former. From 3.5 ms to 6.3 ms, high-intensity currents flowing toward the head appeared and conducted proximally (pink stars). Currents flowing toward the end of the currents marked with pink stars appeared (yellow arrows) and also propagated proximally. From 4.9 ms to 7.9 ms, currents directing caudally appeared and conducted proximally (yellow stars). (For interpretation of the references to colour in this figure legend, the reader is referred to the web version of this article.)

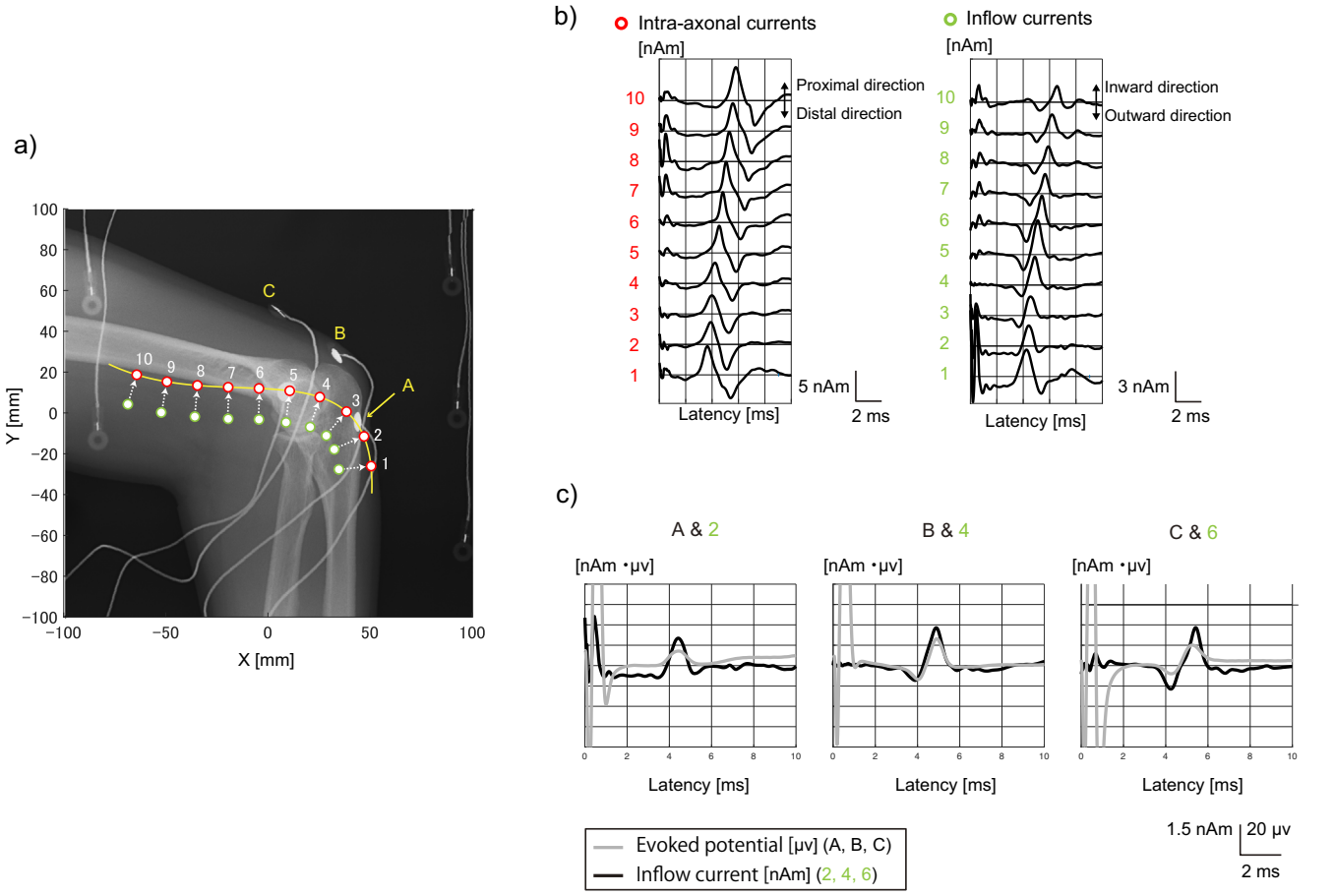

Fig. 8. A time course of the reconstructed currents and the correspondence between evoked potentials and reconstructed currents. (a) The yellow line represents the pathway of the peak intensity of the reconstructed currents marked with pink stars in Fig. 6. Red circles show virtual electrodes on the yellow line placed 15 mm apart. Green circles show virtual electrodes 15 mm away from the yellow line. A, B, and C represent the electrodes used to record evoked potentials. (b) Intra-axonal currents and inflow currents reconstructed at virtual electrodes in (a). Intra-axonal currents are reconstructed at red-circled virtual electrodes and conducted cranially. Inflow currents are reconstructed at virtual electrodes with green crosses and also conducted cranially. Waveforms at the electrodes opposite the green crosses are not shown because some of them are outside the arm. Numbers represent the electrode number shown in (a). (c) Correspondence between evoked potentials and reconstructed inflow currents. Evoked potentials were recorded at the electrodes indicated as A, B, and C (gray waveforms). Inflow currents were picked up from the virtual electrodes labeled with 2, 4, and 6 in (a) and (b) because they are the nearest to the evoked potential electrodes A, B, and C. (For interpretation of the references to colour in this figure legend, the reader is referred to the web version of this article.)

60.3 ± 9.1 m/s (mean ± SD, n = 9), respectively. In addition, the difference in their peak latencies at the medial epicondyle was as small as 0.011 ± 0.29 ms (mean ± SD, n = 9). As we have previously reported, reconstructed inflow currents are believed to represent volume currents flowing into the depolarization site (Fukuoka et al., 2002; Sasaki et al., 2020). Consequently, it is reasonable that the position of the inflow current would be consistent with that of the negative peak of the evoked potential.

The electrophysiological study of the patient with left cubital tunnel syndrome revealed decelerated CVs of SNAPs and CMAPs, which recovered after the surgery. On the intact side of the patient, MNG before surgery showed that both intra-axonal and inflow reconstructed currents propagated at similar CVs. On the affected side, the intra-axonal currents were not distinct, and the inflow currents decelerated and attenuated at the distal point of the medial epicondyle (after 5.0 ms in Fig. 9b; electrodes 5–7 in Fig. 10b). The inflow currents were able to visualize the propagation of the pathological nerve, although the intra-axonal currents could not be evaluated.

As stated in the Introduction, some patients with cubital tunnel syndrome show false-negative results in the electrophysiological examination. A functional imaging technique that can localize lesions that electrophysiological examinations are unable to detect is desired. Given that MNG can visualize intra-axonal currents and volume currents even at curved sites, MNG has the potential to be a complementary functional imaging method to evaluate ulnar nerve entrapment.

Nonetheless, there are some limitations to this study. One is that the depth of the ROI for signal processing was fixed because positional information was acquired from an X-ray image that does not contain information on the exact position of the ulnar nerve. In further studies, we would like to use a magnetic resonance image for positional information, which should improve the accuracy of neural activity localization. Second, dysfunctional ulnar nerve was evaluated in only one patient in this study. We need to examine a greater number of pathological cases before and after the surgical treatment to develop a detailed diagnostic method in MNG.

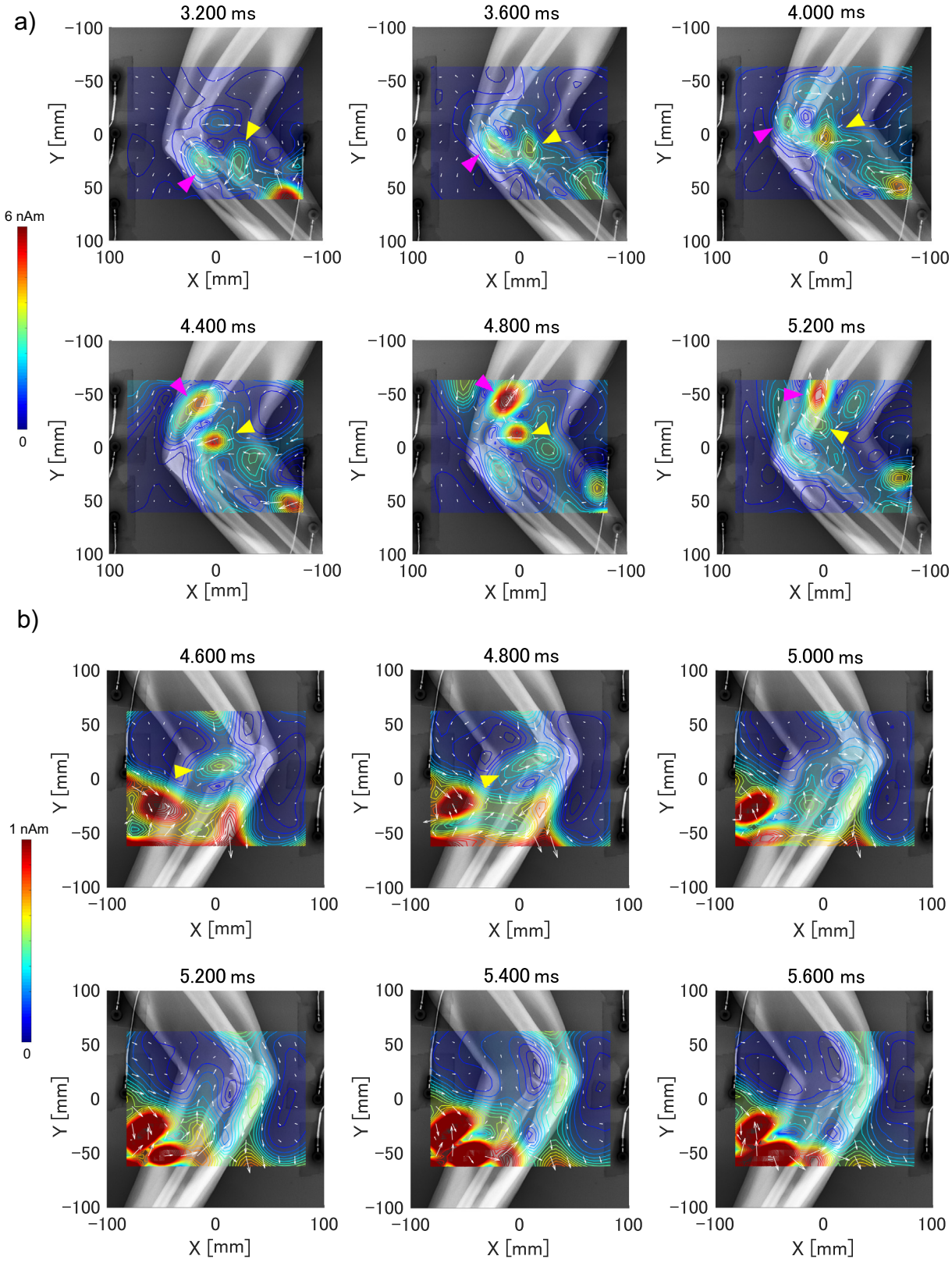

Fig. 9. Spatiotemporal changes in equivalent currents reconstructed with the recursively applied null-steering (RENS) beamformer. A patient with left cubital tunnel syndrome before surgery**.** (a) The right arm (intact side). Reconstructed intra-axonal (pink arrowheads) and inflow (yellow arrowheads) currents propagated proximally. (b) The left arm (affected side). Reconstructed intra-axonal currents are indistinct and inflow currents (yellow arrowheads) disappeared near the medical epicondyle at 5.0 ms. (For interpretation of the references to colour in this figure legend, the reader is referred to the web version of this article.)

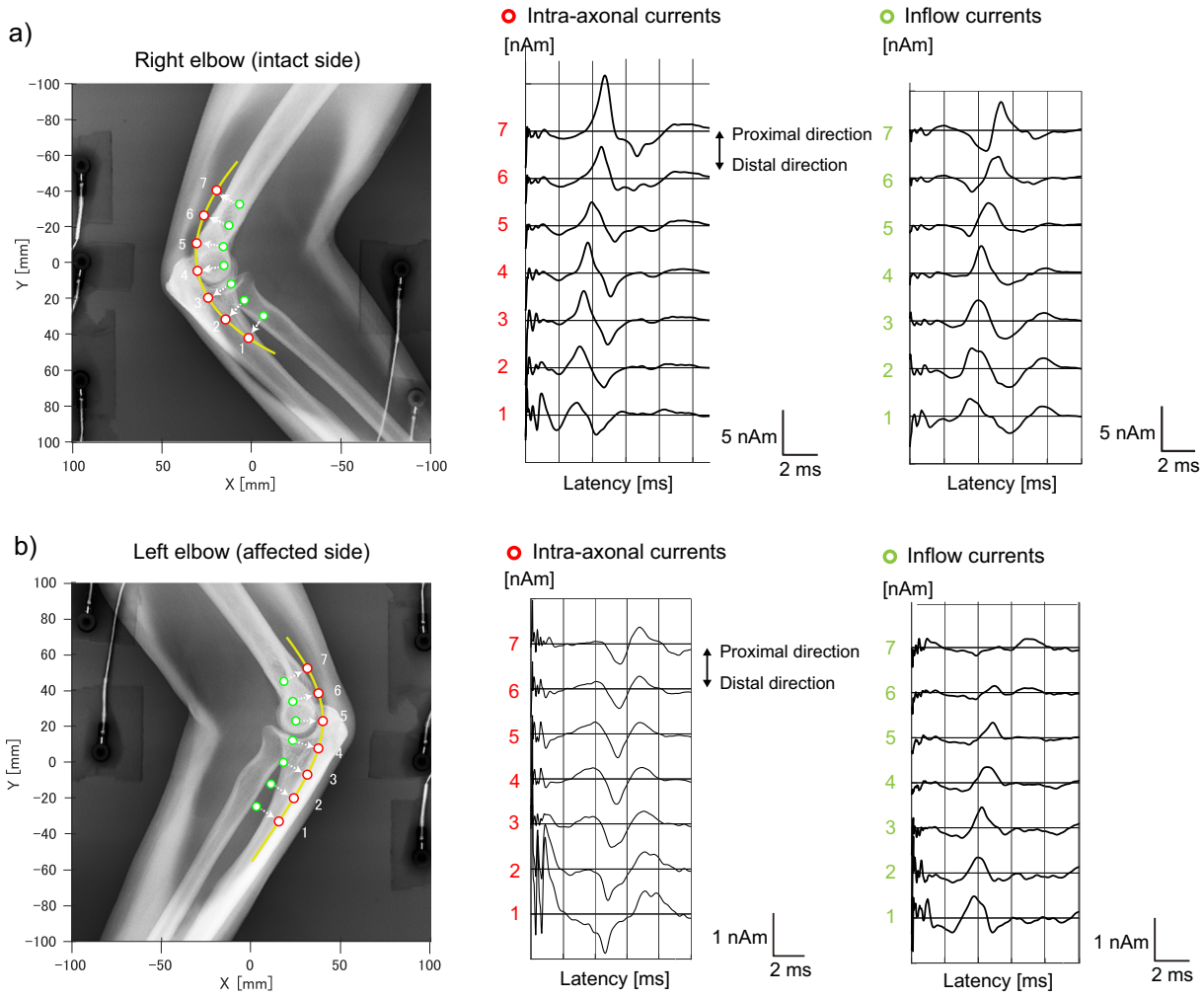

Fig. 10. A time course of the reconstructed currents. A patient with left cubital tunnel syndrome. (a) The right arm (intact side). Intra-axonal and inflow currents propagated proximally. (b) The left arm (affected side). Upward pointing waves of intra-axonal currents are not as clear as in (a). Inflow currents diminished and decelerated at electrodes 5 to 7. Note that the scale of the amplitude is one-fifth that of the right arm.

5. Conclusions

MNG can visualize the neural activity of the ulnar nerve at the elbow as reconstructed currents. Our results show that MNG has the potential be a novel and universal functional imaging technique for evaluating ulnar nerve entrapment, which may boost its diagnostic ability and its use in surgical decision-making.

Funding

This research was supported by Ricoh Company, Ltd. The funding body played no role in study design, data collection and analysis, or preparation of the manuscript.

Declaration of Competing Interest

The authors declare that they have no known competing financial interests or personal relationships that could have appeared to influence the work reported in this paper.

References

Adachi Y, Kawai J, Haruta Y, Miyamoto M, Kawabata S, Sekihara K, et al. Recent advancements in the SQUID magnetospinogram system. Supercond Sci Technol 2017;30(6):063001. https://doi.org/10.1088/1361-6668/aa66b3.

Afra P. The advancement of magnetoneurography. Clin Neurophysiol 2020;131(4):938–9. https://doi.org/10.1016/j.clinph.2019.12.406.

Beekman R, Van Der Plas JPL, Uitdehaag BMJ, Schellens RLLA, Visser LH. Clinical, electrodiagnostic, and sonographic studies in ulnar neuropathy at the elbow. Muscle Nerve 2004;30(2):202–8. https://doi.org/10.1002/mus.20093.

Boone S, Gelberman RH, Calfee RP. The management of cubital tunnel syndrome. J Hand Surg 2015;40(9):1897–904.

Eberlin KR, Marjoua Y, Jupiter JB. Compressive neuropathy of the ulnar nerve: a perspective on history and current controversies. J Hand Surg 2017;42(6):464–9.

Fukuoka Y, Komori H, Kawabata S, Ohkubo H, Shinomiya K. Visualization of incomplete conduction block by neuromagnetic recording. Clin Neurophysiol 2004;115(9):2113–22. https://doi.org/10.1016/j.clinph.2004.03.033.

Fukuoka Y, Komori H, Kawabata S, Ohkubo H, Shinomiya K, Terasaki O. Imaging of neural conduction block by neuromagnetic recording. Clin Neurophysiol 2002;113(12):1985–92.

Greenwald D, Blum LC, Adams D, Mercantonio C, Moffit M, Cooper B. Effective surgical treatment of cubital tunnel syndrome based on provocative clinical testing without electrodiagnostics. Plast Reconstr Surg 2006;117(5):87e–91e. https://doi.org/10.1097/01.prs.0000207298.00142.6a.

Hoshino Y, Kawabata S, Komori H, Ohkubo H, Tomizawa M, Shinomiya K. Three-dimensional neuromagnetic recording in the spinal cord. Int Congr Ser 2005;1278:309–12.

Ishii S, Kawabata S, Tomizawa S, Tomori M, Sakaki K, Shinomiya K, et al. Conductive neuromagnetic fields in the lumbar spinal canal. Clin Neurophysiol 2012;123(8):1656–61. https://doi.org/10.1016/j.clinph.2011.12.014.

Kawabata S, Komori H, Mochida K, Harunobu O, Shinomiya K. Visualization of conductive spinal cord activity using a biomagnetometer. Spine 2002;27(5):475–9. https://doi.org/10.1097/00007632-200203010-00007.

Kumihashi I, Sekihara K. Array-gain constraint minimum-norm spatial filter with recursively updated gram matrix for biomagnetic source imaging. IEEE Trans Biomed Eng 2010;57(6):1358–65. https://doi.org/10.1109/TBME.2010.2040735.

Mackert B-M. Magnetoneurography: theory and application to peripheral nerve disorders. Clin Neurophysiol 2004;115(12):2667–76. https://doi.org/10.1016/j.clinph.2004.07.028.

Pelosi L, Tse DMY, Mulroy E, Chancellor AM, Boland MR. Ulnar neuropathy with abnormal non-localizing electrophysiology: clinical, electrophysiological and ultrasound findings. Clin Neurophysiol 2018;129(10):2155–61.

Sasaki T, Kawabata S, Hoshino Y, Sekihara K, Adachi Y, Akaza M, et al. Visualization of electrophysiological activity at the carpal tunnel area using magnetoneurography. Clin Neurophysiol 2020;131(4):951–7. https://doi.org/10.1016/j.clinph.2019.11.030.

Sekihara K, Kawabata Y, Ushio S, Sumiya S, Kawabata S, Adachi Y, et al. Dual signal subspace projection (DSSP): a novel algorithm for removing large interference in biomagnetic measurements. J Neural Eng 2016;13(3):036007. https://doi.org/10.1088/1741-2560/13/3/036007.

Sekihara K, Nagarajan SS. Electromagnetic brain imaging, a Bayesian perspective. Cham, Switzerland: Springer International Publishing; 2015. Available from: https://www.springer.com/us/book/9783319149462.

Sekihara K, Nagarajan SS. Subspace-based interference removal methods for a multichannel biomagnetic sensor array. J Neural Eng 2017;14(5):051001. https://doi.org/10.1088/1741-2552/aa7693.

Sumiya S, Kawabata S, Hoshino Y, Adachi Y, Sekihara K, Tomizawa S, et al. Magnetospinography visualizes electrophysiological activity in the cervical spinal cord. Sci Rep 2017;7(1). https://doi.org/10.1038/s41598-017-02406-8.

Tomizawa S, Kawabata S, Komori H, Hoshino Fukuoka Y, Shinomiya K. Evaluation of segmental spinal cord evoked magnetic fields after sciatic nerve stimulation. Clin Neurophysiol 2008;119(5):1111–8. https://doi.org/10.1016/j.clinph.2008.01.017.

Ushio S, Hoshino Y, Kawabata S, Adachi Y, Sekihara K, Sumiya S, et al. Visualization of the electrical activity of the cauda equina using a magnetospinography system in healthy subjects. Clin Neurophysiol 2019;130(1):1–11. https://doi.org/10.1016/j.clinph.2018.11.001.

Watanabe T, Kawabata S, Hoshino Y, Ushio S, Sasaki T, Miyano Y, et al. Novel functional imaging technique for the brachial plexus based on magnetoneurography. Clin Neurophysiol 2019;130(11):2114–23. https://doi.org/10.1016/j.clinph.2019.08.006.